Olga Kogtenkova[a], Boris Straumal[a,b], Svetlana Protasova[a], Sadahiro Tsurekawa[c], Tadao Watanabe[c]

[a] Institute of Solid State Physics, Russian Academy of Sciences, Chernogolovka, Russia
[b] Max Planck Institute for Metals Research, Stuttgart, Germany
[c] Laboratory of Materials Design and Interface Engineering, Department of Machine Intelligence and Systems Engineering, Graduate School of Engineering, Tohoku University, Sendai, Japan

# The influence of misorientation deviation on the faceting of Σ3 grain boundaries in aluminium

*Dedicated to Professor Dr. Duk Yong Yoon on the occasion of his 65th birthday*

The faceting of two tilt grain boundaries (GBs) in 99.999 % wt. purity Al bicrystals has been studied. The first GB is a coincidence twin Σ3 <110> GB (Σ is the inverse density of coincidence sites) and the second GB has a misorientation close to the Σ3 <110> with a tilt deviation of about 3 degrees. Orientation of grains along the GB has been controlled with the electron back-scattering diffraction method. The bicrystalline samples were coated with a layer of Sn–Al mixture and annealed at 873 K. Contact angles at the junction of the grain boundary and two solid/liquid interfaces were measured by optical microscopy. The ratio of grain boundary energy and solid/liquid interface energy has been calculated. Wulff–Herring plots and GB phase diagrams were constructed. The formation of smooth edges with rounded rough GB portions was observed in the grain boundary deviating from Σ3 <110>.

**Keywords:** Grain Boundaries; Faceting; Roughening; Al; Misorientation influence; Phase diagrams

## 1. Introduction

Faceting is well known both for surfaces and interfaces, particularly, grain boundaries [1–4]. Recently it started to attract more attention, especially due to the growing role of nanocrystalline materials. Faceting can be considered as a phase transition when the original surface or grain boundary dissociates into flat segments whose energy is less than that of the original surface or grain boundary. Grain boundary faceting proceeds only close to so-called coincidence misorientations. In this case the lattices of both grains form the coincidence site lattice (CSL) characterized by the parameter Σ (reverse density of coincidence sites). In most cases the grain boundary facets lie in the CSL planes with high density of coincidence sites. It has been shown [5] that grain boundaries possess special structure and properties in limited areas of temperature $T$ and misorientation $\theta$ close to a coincidence misorientation, $\theta_\Sigma$. In other words, by increasing $\Delta\theta = |\theta - \theta_\Sigma|$ and $T$, the phase transition "special grain boundary – general grain boundary" proceeds and the grain boundary looses its special structure and properties [6]. This is due to the fact that for the CSLs with low $\Sigma$ the depth of the energy-versus-misorientation profile for the densily packed CSL planes is larger than that of high-$\Sigma$ CSLs. Therefore, due to the temperature-induced disordering the energetically favourable grain boundary positions disappear at lower $T$ for grain boundaries with higher $\Sigma$ [7]. We can expect that at high temperature or increasing $\Delta\theta$ values only the facets with highest density of coincidence sites will appear. It has been observed that GB faceting correlates with the phenomenon of abnormal grain growth in alumina [8], stainless steel [9], silver [10], and nickel-based superalloys [4]. Prof. Yoon with coworkers have demonstrated that above certain temperatures the faceted GBs are absent and abnormal grain growth does not appear [4, 8–10].

## 2. Experimental

For the investigation of grain boundary faceting an Al (99.999 wt.% purity) a bicrystal with a semi-island grain was grown using the modified Bridgman technique. Grain 1 in this bicrystal is semi-surrounded by grain 2 forming a Σ3 <110> tilt grain boundary (Fig. 1). 5 mm thick platelets were cut from the grown bicrystal perpendicular to the growth axis. The bicystalline samples were coated with a layer of Sn–Al mixture and annealed in 80 % Ar + 20 % $H_2$ gas atmosphere at a pressure of $2\times10^{-4}$ Pa and a temperature of 873 K (0.94 of melting temperature $T_m$) for 2 hours. Then the samples were mechanically ground, polished, and etched in 50 % $HNO_3$ + 47 % HCl + 3 % HF solution. To determine the ratio between grain boundary energy, $\sigma_{GB}$, and solid/liquid interface energy, $\sigma_{SL}$, the contact angle $\alpha$ was measured in the triple point of the grain

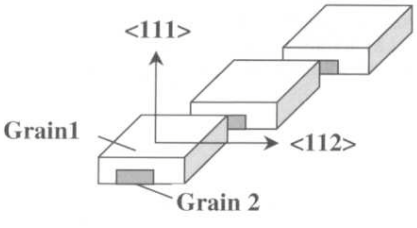


Fig. 1. Schematic view of the bicrystal samples.

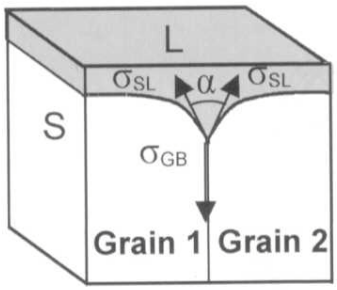


Fig. 2. Scheme of the equilibrium contact between the grain boundary in the solid phase **S** and the liquid phase **L** (incomplete wetting).

boundary and the two solid/liquid interfaces (Fig. 2). The contact angle $\alpha$ and the geometry of the facets were analysed and recorded in bright and dark field in a light microscope (Figs. 3 and 4). The $\sigma_{GB}/\sigma_{SL}$ ratio was calculated as follows: $\sigma_{GB} = 2\sigma_{SL}\cos(\alpha/2)$. The cross-sections of bicrystals containing exact Σ3 and "deviated" grain boundaries are shown in Fig. 4.

The electron back-scattering diffraction (EBSD) method was used to determine the individual grain orientation in the Al bicrystals and the grain boundary shape in the as-grown bicrystals. The EBSD method permits observation of the sample microstructure and determination of the individual grain orientation in the same experiment. The EBSD patterns were measured using a Hitachi S-4200 scanning electron microscope. The spatial resolution in EBSD reaches 50 nm. We determined the individual grain orientation using the integrated software package for semi-automated fit procedure for indexing of the EBSD patterns. For the first type of samples the misorientation deviation from exact Σ3 <110> was less then 1° along grain boundary. For the second one this deviation was about 3° along the grain boundary. Remarkably, there were no triple junctions in the corners of the semi-surrounded grain.

## 3. Results and discussion

The main goal of the current work was to study the influence of misorientation deviation $\Delta\theta$ on the grain boundary faceting. Main facets in exact Σ3 and deviated Σ3 grain boundaries are symmetric Σ3 twins $\{111\}_1/\{111\}_2$. They correspond also to the (100) plane of Σ3 CSL and will be called below as $(100)_{\Sigma3CSL}$ facets. Facets other than $(100)_{\Sigma3CSL}$ facets were observed only in the exact Σ3 grain boundary (Table 1). They form angles of 82° and 56° with the $\{111\}_1/\{111\}_2$ [or $(100)_{\Sigma3CSL}$] facet. The section of Σ3 CSL perpendicular to the <110> axis is shown in Fig. 5. The most closely-packed CSL planes are shown together

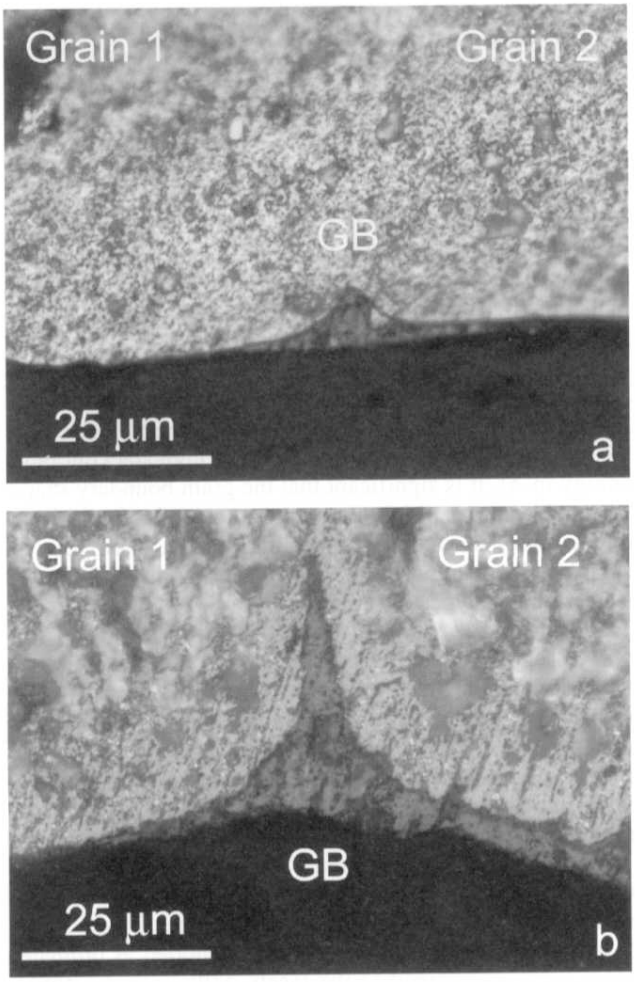


Fig. 3. The contact angle $\alpha$ of the Σ3 grain boundary at different facets: (a) $(100)_{\Sigma3CSL}$ facet; (b) 9R facet.

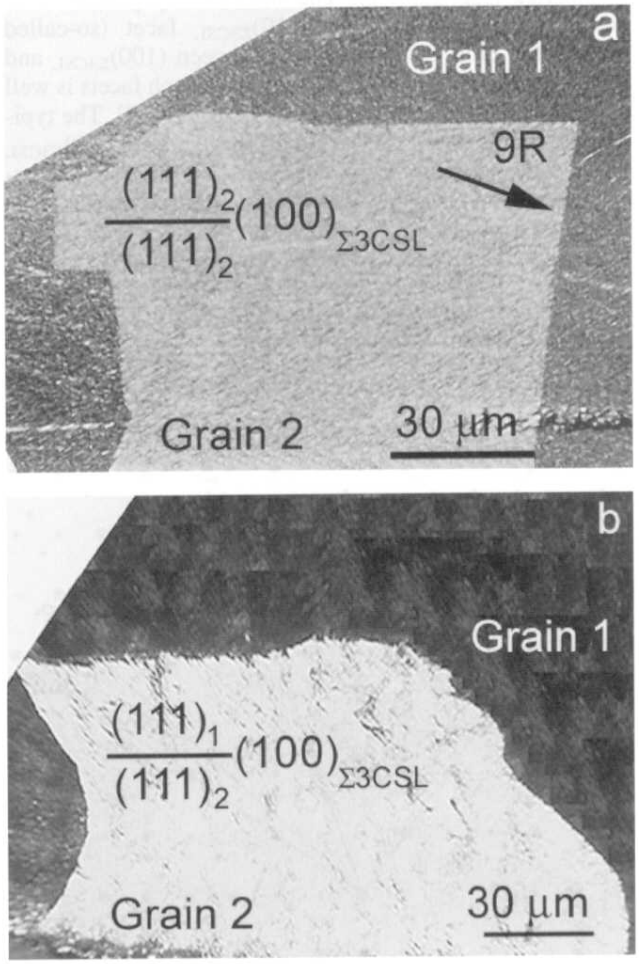


Fig. 4. Light micrographs showing the cross-sections of bicrystals containing (a) an exact Σ3 grain boundary and (b) a grain boundary with 3° deviation.

Table 1. The presence of different facets at different $\Delta\theta$ values.

| Grain boundary misorientation | Facet | Orientation angle $\varphi$ |
|---|---|---|
| exact Σ3 | $(100)_{\Sigma 3CSL}$ | 0° |
| | 9R | 82° |
| | $(110)_{\Sigma 3CSL}$ | 56° |
| deviating Σ3 | $(100)_{\Sigma 3CSL}$ | 0° |

with respective planes for the lattices 1 and 2 forming the CSL. It can be easily seen that the facet having an angle of 56° with the $(100)_{\Sigma 3CSL}$ facet is the $\{100\}_1/\{122\}_2$ [or $(110)_{\Sigma 3CSL}$ facet]. However, the facet forming an angle of 82° with the $(100)_{\Sigma 3CSL}$ facet is not a CSL facet.

In Fig. 6 the Wulff–Herring plot is shown for the exact Σ3 and deviated Σ3 grain boundaries at 873 K. The Wulff–Herring plot was constructed using the $\sigma_{GB}/\sigma_{SL}$ ratios measured by optical microscopy. The most important results following from the comparison of Figs. 6a and b is that by increasing $\Delta\theta$, only the $(100)_{\Sigma 3CSL}$ facet remains in the equilibrium shape, and the two other facets become unstable. Rough rounded GB portions appear instead.

The energy of the symmetric Σ3 twin $\{111\}_1/\{111\}_2$ or $(100)_{\Sigma 3CSL}$ facet is very low. These facets are very stable and are observed both in exact Σ3 and deviated grain boundaries (see Table 1). The next-closely packed CSL plane is $\{211\}_1/\{211\}_2$ or $(010)_{\Sigma 3CSL}$ facet (so-called asymmetric twin GB). The angle between $(100)_{\Sigma 3CSL}$ and $(010)_{\Sigma 3CSL}$ facets is 90°. The presence of such facets is well documented for Al, Au, $AuCu_3$, and Ge [11–14]. The typical rectangular twin plates with $(100)_{\Sigma 3CSL}$ and $(010)_{\Sigma 3CSL}$ facets can be seen, for example, in Au thin films [12]. However, the twin plates in Cu and Ag are not rectangular. The end facet forms an angle of 82° with the $\{111\}_1/\{111\}_2$ or $(100)_{\Sigma 3CSL}$ facets [15, 16]. TEM studies revealed that this 82° facet has a so-called 9R structure forming a plate of bcc grain boundary phase in the fcc matrix [17–20]. Such $(100)_{\Sigma 3CSL}$ and 82° 9R facets in the Σ3 twin plate are clearly

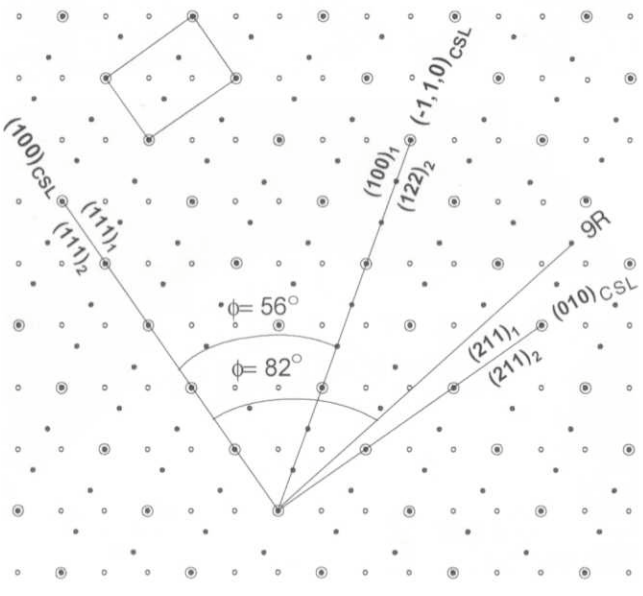


Fig. 5. Section of the Σ3 CSL perpendicular to the {110} tilt axis with the CSL unit cell and positions of various CSL and non-CSL facets.

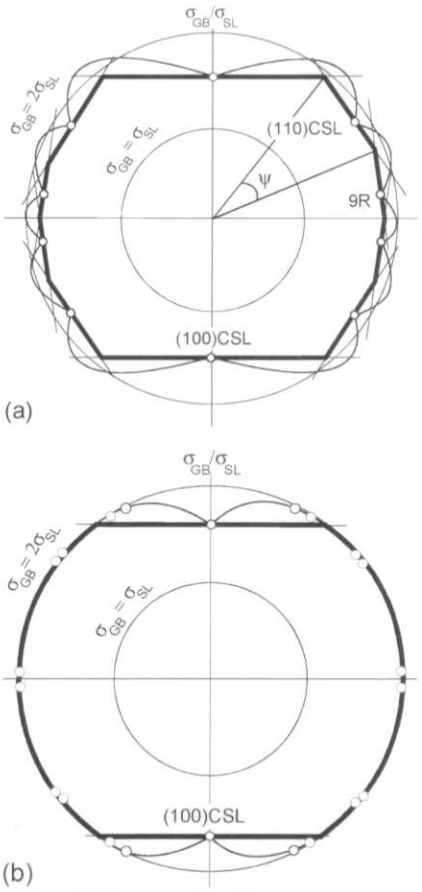


Fig. 6. Wulff–Herring plots for (a) the exact and (b) the deviated Σ3 grain boundaries at 873 K.

seen also in our samples in Fig 4a. Moreover, the analysis of the literature shows that the 82° 9R facet appears in Cu only at high temperatures. At low temperatures the "normal" 90° $(010)_{\Sigma 3CSL}$ facets are present in Cu [20]. The 82° 9*R* facet appears instead of the 90° $(010)_{\Sigma 3CSL}$ facet. In our samples the 82° 9R facet is present in the samples with exact Σ3 grain boundary. The 90° $(010)_{\Sigma 3CSL}$ facet was absent in both types of samples in our studies. The stability of the 9R facet may be connected with a very high stacking fault energy in Al. It is significant that the grain boundary shape was stable at very high temperature (close to the melting temperature) during long annealing time in both types of samples. It is supposed that this shape is an equilibrium shape for both types of samples.

The facet 56° with the $\{100\}_1/\{122\}_2$ [or $(110)_{\Sigma 3CSL}$] was observed for the exact Σ3 boundary and was not detected for the deviated grain boundary. This facet remains stable in the exact Σ3 grain boundary even after long annealing time. With increasing $\Delta\theta$ the formation of rounded rough GB portions was observed. It can be supposed that with increasing of $\Delta\theta$ the length ratio of faceted and rounded rough GB portions decreases.

In Fig. 7 the phase diagram for Σ3 facets is shown according to the approach proposed in [21, 22] for the equilibrium crystal shape. Instead of temperature the deviation from coincidence misorientation $\Delta\theta$ is plotted as ordinate. Open rings correspond to the facets. Filled squares correspond to the rough GB portions. The stability field of the $(100)_{\Sigma 3CSL}$ facet exists both at exact coincidence and $\Delta\theta =$

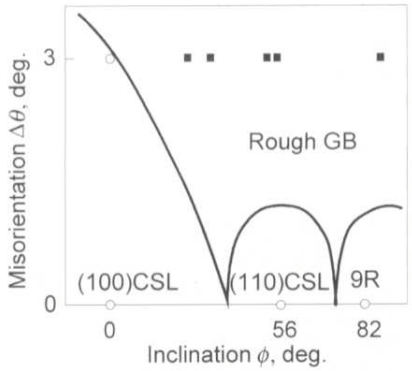


Fig. 7. Phase diagram for Σ3 facets in Al according to the approach [21, 22] for the equilibrium crystal shape in coordinates "deviation from coincidence misorientation $\Delta\theta$" – "inclination $\varphi$". Open rings correspond to the facets. Filled squares correspond to the rough GB portions.

3°. However, the stability field of the $(100)_{\Sigma 3CSL}$ facet becomes narrower with increasing $\Delta\theta = 3°$. The stability fields for $(110)_{\Sigma 3CSL}$ and 9R facets are restricted and exist only at low $\Delta\theta$ and do not extend to $\Delta\theta = 3°$. They transform into rounded rough GB portions. Therefore, starting from certain $\Delta\theta$, the equilibrium shape of the Σ3 GB in Al becomes similar to that in Mo (metal with body-centred cubic lattice) [23].

## 5. Conclusions

1. The exact Σ3 <110> tilt GB and the GB deviating by 3° from exact Σ3 become faceted upon annealing at 0.94 $T_m$.
2. The exact Σ3 <110> tilt GB is completely faceted. The $(100)_{\Sigma 3CSL}$, $(110)_{\Sigma 3CSL}$ facets, and the non-CSL 82° 9R facet are observed. These facets form sharp edges.
3. The 3°-deviated GB is partly faceted, partly rough. Only $(100)_{\Sigma 3CSL}$ facets forming smooth edges with rough GB portions are observed.
4. Wulff–Herring plots were constructed on the basis of GB energy measurements for the various facets for both exact and deviated GBs.
5. For the exact Σ3 GB of the $(100)_{3CSL}$, $(110)_{\Sigma 3CSL}$, and the non-CSL 9R facets are stable. Upon increasing $\Delta\theta$, the $(110)_{\Sigma 3CSL}$ and the non-CSL 9R facets disappear from the equilibrium shape of Σ3 GB. I.e., the roughening temperature for the $(110)_{\Sigma 3CSL}$ and 9R facets is higher than $T_m$ for exact Σ3 GB and lower than $T_m$ for the deviated GB.

These investigations were partly supported by the German Federal Ministry for Education and Research (WTZ-Project RUS 04/014), INTAS (contract 03-51-3779), the Russian Foundation for Basic Research RFBR (contracts 04-03-32800, 03-02-16947 and 03-02-04000) and the NATO Linkage grant (contract PST.CLG.979375). Fruitful discussions with Profs. E. Rabkin, W. Gust, and Dr. W. Sigle are acknowledged.

## References

[1] M. Yoon, S.G.J. Mochrie, M.V. Tate, S.M. Gruner, E.F. Eikenberry: Surf. Sci. 411 (1998) 70.
[2] S.B. Lee, D.Y. Yoon, M.F. Henry: Acta mater. 48 (2000) 3071.
[3] R. Hild, C. Seifert, M. Kammler, F.J. Meyer zu Heringdorf, M. Horn-von-Hoegen, R.A. Zhachuk, B.Z. Olshanetsky: Surf. Sci. 512 (2002) 117.
[4] S. Song, S.G.J. Mochrie: Phys. Rev. B 51 (1995) 10068.
[5] B.B. Straumal, L.S. Shvindlerman: Acta metall. 33 (1985) 1735.
[6] E.L. Maksimova, L.S. Shvindlerman, B.B. Straumal: Acta metall. 36 (1988) 1573.
[7] A.A. Zisman, V.V. Rybin: Poverkhnost' 7 (1982) 87 (in Russian).
[8] J.M. Paik, Y.J. Park, M.S. Yoon, J.H. Lee, Y.C. Joo: Scripta mater. 48 (2003) 683.
[9] J.S. Choi, D.Y. Yoon: ISIJ International 41 (2001) 478.
[10] J.B. Koo, D.Y. Yoon: Metall. Mater. Trans. A 32 (2001) 469.
[11] J.M. Pénisson, U. Dahmen, M.J. Mills: Phil. Mag. Lett. 64 (1991) 277.
[12] P.J. Goodhew, T.Y. Tan, R.W. Balluffi: Acta metall. 26 (1978) 557.
[13] F.D. Tichelaar, F.W. Schapink: J. Phys. Paris 49, C 5 (1988) 293.
[14] A. Bourret, J.J. Bacmann: Inst. Phys. Conf. Series 78 (1985) 337.
[15] T. Muschik, W. Laub, M.W. Finnis, W. Gust: Z. Metallkd. 84 (1993) 596.
[16] A. Barg, E. Rabkin, W. Gust: Acta metall. mater. 43 (1995) 4067.
[17] U. Wolf, F. Ernst, T. Muschik, M.W. Finnis, H.F. Fischmeister: Phil. Mag. A 66 (1992) 991.
[18] F. Ernst, M.W. Finnis, D. Hoffmann, T. Muschik, U. Schönberger, U. Wolf: Phys. Rev. Lett. 69 (1992) 620.
[19] D. Hofmann, M.W. Finnis: Acta metall. mater. 42 (1994) 3555.
[20] B.B. Straumal, S.A. Polyakov, E. Bischoff, W. Gust, E.J. Mittemeijer: Interface Sci. 9 (2001) 287.
[21] C. Rottman, M. Wortis: Phys. Rev. B 24 (1981) 6274.
[22] C. Rottman, M.Wortis: Phys. Rev. B 29 (1984) 328.
[23] B.B. Straumal, V.N. Semenov, O.A. Kogtenkova, T. Watanabe: Phys. Rev. Lett. 192 (2004) 196101.

(Received July 19, 2004; accepted September 16, 2004)

Correspondence address

Prof. Dr. Boris Straumal
Institute of Solid State Physics, Russian Academy of Sciences
Chernogolovka, 142432 Russia
Tel.: +7 916 676 8673
Fax: +7 095 238 2326
E-mail: straumal@issp.ac.ru and straumal@mf.mpg.de